

Detecting phase transitions in- and out-of-equilibrium via single-particle covariance matrices

Miguel M. Oliveira*

CeFEMA, Instituto Superior Técnico, Universidade de Lisboa Av. Rovisco Pais, 1049-001 Lisboa, Portugal

Pedro Ribeiro†

*CeFEMA, Instituto Superior Técnico, Universidade de Lisboa Av. Rovisco Pais, 1049-001 Lisboa, Portugal and
Beijing Computational Science Research Center, Beijing 100193, China*

Stefan Kirchner‡

*Zhejiang Institute of Modern Physics, Zhejiang University, Hangzhou, Zhejiang 310027, China and
Zhejiang Province Key Laboratory of Quantum Technology and Device, Zhejiang University, Hangzhou 310027, China*

(Dated: November 2, 2021)

In this letter we address the problem of detecting phase transitions without prior knowledge of a suitable order parameter. To this end, we propose a notion of metric based on the distance between single-particle covariance matrices. Unlike the well-known fidelity susceptibility, this quantity is accessible to commonly employed numerical techniques and can potentially serve as a versatile instrument to identify phase transitions beyond Landau's paradigm.

In particular, we demonstrate that one choice of metric, which we dubbed single-particle affinity and that coincides with the fidelity for quadratic models can identify non-equilibrium phase transitions. This is shown for a boundary-driven fermion chain under Markovian dissipation, that escapes Landau's framework. We also apply this method to a fermion ladder and find a rather rich phase diagram, contrary to what would be expected from preceding related work on spin ladders.

I. INTRODUCTION

Quantum systems out of equilibrium can exhibit a wide variety of phenomena ranging from the usual symmetry-based phase transitions [1–9] to the more exotic behavior, such as mixed-order phase transitions [10–12] or time crystallinity [13, 14], with no equilibrium counterpart. While conditions for reaching and maintaining equilibrium are well established, a full understanding of matter out of equilibrium is still lacking. This includes the general description of quantum phase transitions far from equilibrium where a linear-response based approach is no longer valid. Even the detection of phase transitions away from equilibrium, where thermodynamic minimization principles no longer apply, can be challenging, in particular when candidate order parameters are a priori unknown.

This difficulty is already present in the so-called Markovian approach to open systems, where the time scales of the environment are taken to be much faster than those of the system. This Markovian limit has recently received considerable attention [15] both for its physical relevance and because it represents a substantial simplification with respect to generic open many-body quantum systems. Additionally, in one spatial dimension, non-equilibrium steady-states (NESS) of Markovian systems can be effectively parameterized by Matrix Product Operators (MPO) [16, 17]. This approach led to a number of important developments in the transport properties of quantum systems and in particular spin chains. For a boundary driven Heisenberg XXZ chain, *e.g.*, it

helped establish the NESS phase diagram [18–26], with further support coming from a series of exact results [27–31].

However, for more generic cases, where analytical results are not readily available, it can be rather difficult to determine phase boundaries if a suitable order parameter is unknown. There are some "all purpose" quantities, like the Fidelity susceptibility [32–36], which are in principle able to detect phase transitions in the absence of preliminary knowledge. But these quantities are forbiddingly difficult to compute in practice using current numerical methods as they require information about the full density matrix. This makes these quantities inaccessible to Monte Carlo methods and cancels the advantage of exponential compression exploited by variational methods such as DMRG.

In this letter, we propose to use a class of single-particle observables to detect phase transitions. These quantities are derived from a notion of proximity between covariance matrices, similarly to the Fidelity which is related to a distance between density matrices. Being dependent solely on single-particle quantities they are efficiently accessible by typically employed numerical methods. In what follows, we focus on a quantity we dubbed single-particle affinity (SPA).

We demonstrate the usefulness of the SPA through the study of a model with a well-established NESS phase diagram.

As a further test, we apply the SPA as an "all purpose" detector of phase transitions using it to investigate a boundary-driven fermionic ladder whose NESS phase

diagram has not been reported so far. As it turns out, this phase diagram is rather rich, contrarily to naive expectations. Guided by the SPA result, we also confirm these findings through a careful analysis of the finite size scaling of the current.

Single-particle affinity. — In order to assess the far-from-equilibrium behavior of electronic matter, we note that for a fermionic system all single-particle observables can be obtained from the covariance matrix $\Sigma = \langle \mathbf{C} \mathbf{C}^\dagger \rangle$, where $\mathbf{C} = (c_1, c_2, \dots, c_1^\dagger, c_2^\dagger, \dots)^T$ is a Nambu-vector. Here, Σ is Hermitian, $\Sigma^\dagger = \Sigma$ and respects charge conjugation symmetry, *i.e.*, $\Sigma = \tau_x (1 - \Sigma^T) \tau_x$, with τ_x being the x Pauli matrix acting in Nambu space.

It is well known that in equilibrium, the order parameter of, *e.g.*, charge-, spin-density waves or superconducting phases is constructed from single-particle operators, which can even signal topological phase transitions for which a local order parameter cannot be defined. Even far-from-equilibrium, where a symmetry-breaking order parameter is often not available, the covariance matrix may still encode important information about phase changes in the non-equilibrium steady-state.

We explore the ability of the covariance matrix to identify phase transitions by studying a suitable measure of distance between covariance matrices $D_{\mathcal{A}}^2(\Sigma_1, \Sigma_2) = 2 - 2\sqrt{\mathcal{A}(\Sigma_1, \Sigma_2)}$ where \mathcal{A} is a quantity we will refer to as SPA

$$\mathcal{A}(\Sigma_1, \Sigma_2) = \frac{\det \left[\mathbf{1} + \sqrt{(\Sigma_1^{-1} - \mathbf{1})(\Sigma_2^{-1} - \mathbf{1})} \right]}{\sqrt{\det [\Sigma_1^{-1}] \det [\Sigma_2^{-1}]}}. \quad (1)$$

$D_{\mathcal{A}}$ obeys all the properties of a metric, thus providing a sensible notion of affinity between two states (see [37]-S1). For two quadratic density matrices \mathcal{A} coincides with the fidelity F , *i.e.*, $F(\rho_1, \rho_2) = \mathcal{A}(\Sigma_1, \Sigma_2)$, where $F(\rho_1, \rho_2) = (\text{Tr} \sqrt{\sqrt{\rho_1} \rho_2 \sqrt{\rho_1}})^2$ and $\Sigma_i = \text{Tr} [\mathbf{C} \mathbf{C}^\dagger \rho_i]$ (see [37]-S1). Therefore, in the quadratic case $D_{\mathcal{A}}(\Sigma_1, \Sigma_2)$ reduces to the Bures distance $D_{\mathcal{B}}^2(\rho_1, \rho_2) = 2 - 2\sqrt{F(\rho_1, \rho_2)}$ [38–41].

As the quantities entering Σ are, at least in principle, straightforwardly accessible in most numerical and approximation methods, detecting phase-transitions based on this quantity is of great practical purpose. This is in contrast to the fidelity whose numerical calculation, for an interacting system, is in general not feasible. Thus, $D_{\mathcal{A}}$ could serve as an efficient instrument to screen for phase changes in general models of NESS.

By construction, \mathcal{A} reproduces previous results for non-interacting fermionic systems based on F [33]. We will demonstrate the usefulness of \mathcal{A} for steady-state phase transitions of interacting systems. This is accomplished by studying a generalized linear response suscep-

tibility associated with \mathcal{A} and defined through

$$\mathcal{A}[\Sigma(\lambda), \Sigma(\lambda + d\lambda)] = 1 - \sum_{i,j} \chi_{\mathcal{A}}^{i,j}(\lambda) \frac{d\lambda_i d\lambda_j}{2} + O(d\lambda^3), \quad (2)$$

where λ parametrizes the non-equilibrium steady-state.

We consider two boundary-driven models with Markovian reservoirs that allow injection or removal of electrons (see Figs.1-(a) and 3-(b)). The Markovian evolution is described by a Lindblad equation [42, 43]

$$\partial_t \rho = \mathcal{L}(\rho), \quad (3)$$

where ρ is the density matrix of the system. The Lindblad operator \mathcal{L} is given by

$$\mathcal{L}(\rho) = -i[H, \rho] + \sum_{\alpha} \left[W_{\alpha}^{\dagger} \rho W_{\alpha} - \frac{1}{2} \{W_{\alpha}^{\dagger} W_{\alpha}, \rho\} \right]. \quad (4)$$

Here $[\]$ and $\{ \}$ denote commutator and anti-commutator respectively, while W_l are the so-called jump operators which encode the system-reservoir couplings. In Eq. (4), the first term is responsible for the unitary part of the time evolution and the second describes driving and dissipation.

The first system we consider is the $t - V$ model for spinless electrons on a chain, where we demonstrate that \mathcal{A} reproduces the previously known phase diagram. The Hamiltonian of this $t - V$ model is given by

$$H = \sum_{\langle i,j \rangle} \left[-t c_i^{\dagger} c_j + \frac{V}{2} \left(n_i - \frac{1}{2} \right) \left(n_j - \frac{1}{2} \right) \right], \quad (5)$$

where c_i^{\dagger}, c_i are the creation and annihilation operators on site i , $n_i = c_i^{\dagger} c_i$, t is the hopping amplitude, set to unity in the following, V is a nearest-neighbour density-density interaction and L the length of the system. Here, $i = 1, \dots, L$, and the nearest neighbour summation, $\sum_{\langle i,j \rangle}$, is restricted to $j = i \pm 1$, where open boundary conditions are assumed. The jump operators in this case are

$$W_{l,-} = \sqrt{\Gamma_l \frac{1 - \eta_l}{2}} c_l, \quad W_{l,+} = \sqrt{\Gamma_l \frac{1 + \eta_l}{2}} c_l^{\dagger}, \quad (6)$$

where $l = 1, L$ labels the end points of the chain, Γ_l is the injection/removal rate for the l^{th} reservoir and the bias η_l specifies the associated imbalance between particle injection and removal. Thus, the summation in Eq.(4) is performed over $\alpha = (l, \pm)$. In what follows we set $\Gamma_l = 1$ and reduce the bias to a single parameter $\eta_1 = -\eta_L = \eta$. This system is equivalent to the boundary-driven XXZ chain studied in Refs. [18–26, 29, 30].

The steady-state phase diagram of the boundary-driven $t - V$ chain, sketched in Fig.1-(a), is reproduced in Fig.1-(b). Fig.1-(c) shows the real space occupations, $n_r = c_r^{\dagger} c_r$. In the diffusive regime, away from

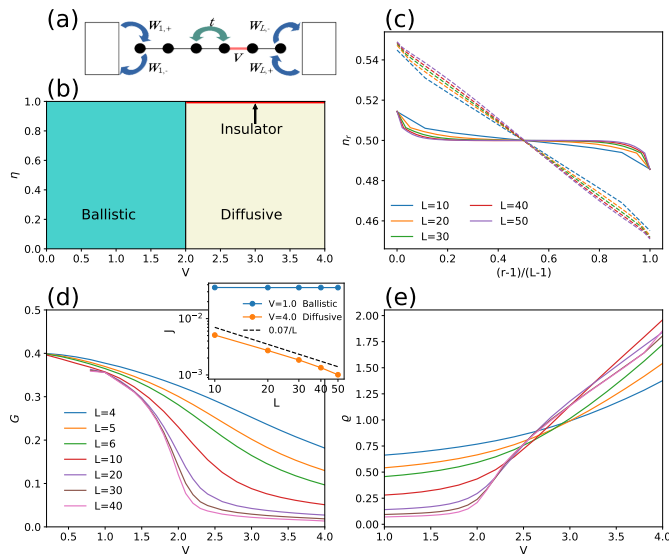


FIG. 1. (a) Scheme of the fermion chain model. (b) Phase diagram of the model, showcasing a ballistic, diffusive and insulating regimes. (c) Comparison of the real space occupations between the ballistic phase at $V = 1.0$ (continuous) and the diffusive at $V = 4.0$ (dashed). (d) G as a function of V for different system sizes. The inset shows the current's dependence with L for the different regimes, with the dashed line being a guide for the eyes delineating the diffusive behavior. (e) ϱ as a function of V for different system sizes. (c), (d) and (e) were obtained for $\eta = 0.1$.

the boundaries, the density profile is linear in r , *i.e.*, $n_r - 1/2 \propto \eta(1/2 - r/L)$. This is in contrast to the ballistic case where the density profile is position independent away from the leads [18–20]. The diffusion constant is then defined as $J = -D(V, \eta) \frac{\partial n_r}{\partial r}$, and becomes independent of η for small η .

Fig.1-(d) (inset) depicts the dependence of the current $J(L) = -it \langle c_i^\dagger c_{i+1} - \text{h.c.} \rangle$ on L in each of the phases: the ballistic phase, for $V < V_c = 2$, where $J(L)$ is L independent; the diffusive regime where $J(L) \propto L^{-1}$; and the insulating phase (not shown) for $\eta = 1$ and $V > V_c$ where $J(L)$ vanishes exponentially with L [20].

This leads us to the identification of suitable order parameters for the various regimes. In the ballistic phase, we make use of the L -independence of the current and take the conductance $G = J/\eta$, where η takes the place of the applied bias, as shown in Fig.1-(d) (main panel). In the diffusive regime we define an effective non-linear resistivity constant as $J = \eta/R$, where $R = \varrho L$ is the induced resistance. $\varrho = \eta/(JL)$, the resistivity, then serves as an order parameter. Fig.1-(e) shows that ϱ vanishes as $L \rightarrow \infty$ for $V < V_c$.

The second case we consider is that of an interacting two-leg ladder whose NESS behavior has not been addressed before. The system is described by Eq. (5), with $i = (r, \tau)$, where $r = 1, \dots, L$ labels the rungs and $\tau = 1, 2$

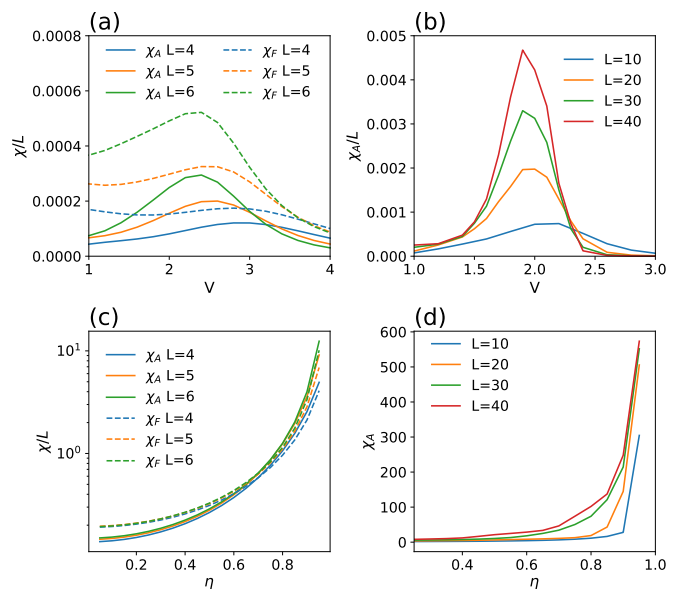


FIG. 2. Results obtained for the fermion chain model. (a), (b) Affinity susceptibility per degree of freedom as a function of the interaction V for different system sizes at $\eta = 0.1$, detecting the presence of the ballistic-diffusive transition. (a) compares this with the fidelity susceptibility, which exhibits compatible behavior. (c) and (d) show the affinity susceptibility as a function of the bias η for $V = 4$, with (c) also comparing it with the fidelity susceptibility. Results for (a) and (c) were obtained with exact diagonalization using the perturbations $\delta V = 0.01$ and $\delta \eta = 0.01$ respectively, and (b) and (d) with MPS techniques using $\delta V = 0.2$ and $\delta \eta = 0.05$.

the legs. The jump operators, located at the ends of the ladder, are given by Eq. (6) with $l = (r = 1, L; \tau = 1, 2)$, $\eta_{(r=1, \tau=1, 2)} = -\eta_{(r=L, \tau=1, 2)} = \eta$ and $\Gamma_{(r=1, L, \tau=1, 2)} = 1$.

Somewhat similar systems featuring spins on a ladder were studied by Žnidarič [44, 45]. The Hubbard model which can also be seen as a ladder system with the spin indexing the legs has been widely studied [46–48]. It was found that, in contrast to the chain, the ballistic regime appears to be absent for locally coupled reservoirs under symmetric driving. Generic diffusive behaviour was also found for closed spin ladders in the linear-response regime using quantum typicality arguments [49].

We analyse the steady-state properties of the models defined above using techniques for open systems based on Matrix Product States (MPS) which has been shown to yield reliable results for this class of boundary-driven problems [16, 17]. Starting in the infinite temperature state, we time evolve the system according to Eq.(4) using the t-DMRG algorithm [50] until it reaches the steady state. Details of the implementation and convergence of the algorithm are provided in the supplemental material [37]-S3, S4.

Results. — Fig.2-(a), (b) show the SPA susceptibility, χ_A^{VV} , in Eq.2 for the well established ballistic-diffusive

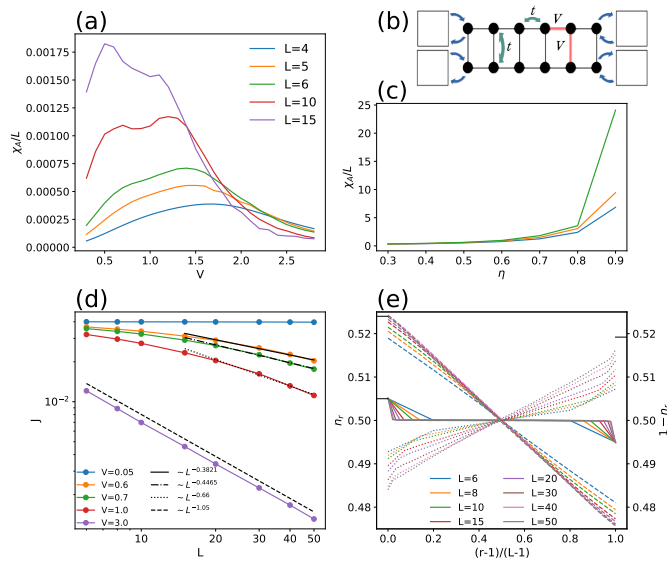


FIG. 3. Results obtained for the fermion ladder model. (a) Affinity susceptibility per degree of freedom as a function of the interaction V for different system sizes at $\eta = 0.1$, detecting a transition from a ballistic to a diffusive phase, while crossing an intermediate super-diffusive regime. $\delta V = 0.2$ was the perturbation considered. (b) Scheme of the fermion ladder model. (c) Affinity susceptibility as a function of the bias η for different system sizes at $V = 3.0$, with a perturbation of $\delta\eta = 0.1$. (d) Comparison of the L dependence of the current for the different regimes, with $\eta = 0.05$. The straight lines serve as guides to the eye for the power-law behavior of the diffusive and super-diffusive phases. (e) Comparison of the real space occupations between the ballistic phase at $V = 0.05$ (continuous), the diffusive at $V = 3.0$ (dashed) and the super-diffusive at $V = 0.7$ (dotted), all for $\eta = 0.05$. For the super-diffusive case (dotted) we showed $1 - n_r$ to avoid overlapping the curves.

transition of the chain model. Fig.2-(a) also depicts a comparison with the fidelity susceptibility, χ_F^{VV} , for small systems sizes, obtained by exact diagonalization. Clearly χ_F^{VV} signals the presence of a transition, at V_c , of the infinite system already at reduced system sizes and χ_A^{VV} tracks the behavior of χ_F^{VV} near the transition.

For larger system sizes, the finite-size scaling analysis shown in Fig.2-(b) confirms that χ_A^{VV} can be used to effectively detect the steady-state phase transition.

Fig.2-(c) shows a similar comparison between $\chi_F^{\eta\eta}$ and $\chi_A^{\eta\eta}$ showing that both quantities increase towards the $\eta = 1$ critical line where the system is insulating, see Fig.1. Fig.2-(d) reaffirms this behavior for larger systems sizes. A similar increase of the $\chi_A^{\eta\eta}$ while approaching the $\eta = 1$ line is also seen for $V < V_c$, which indicates that the nature of the $\eta = 1$ ballistic state is also critical with respect to the $\eta < 1$ phase (see [37]-S2).

We now turn to a discussion of the boundary driven fermionic ladder, Fig.3-(b).

Motivated by the results of Refs [44–46] one may ex-

pect that the phase diagram of this model would feature only diffusive behavior.

This expectation, however, is in sharp contrast to the behavior of the χ_A^{VV} vs. V , shown in Fig.3-(a) for different L . As L increases, this quantity develops a two-peak structure hinting at the existence of two phase transitions, located at V_{c1} and V_{c2} , and a much richer phase diagram.

In what follows we investigate the properties of the different regimes which does demonstrate the predictive power of Σ . In Fig.3-(d), we show J as a function of L . Surprisingly, in addition to the ballistic and diffusive phases for small and large V respectively, we find a super-diffusive regime at intermediate V for which $J \propto L^{-\nu}$, with $0 < \nu < 1$.

Fig.3-(e) shows the density profiles for the three phases in one of the rows of the ladder. The profiles in the ballistic and diffusive regimes have a behaviour which is similar to the corresponding phases of the chain. For the super-diffusive phase, the density profile also seems to depend linearly in r near the middle of the system.

Similarly to what happens for the chain, the $\eta = 1$ here is critical for all values of V , see Fig.3-(c) for the diffusive regime and [37]-S2 for an additional value of V .

Fig.4-(a) depicts the phase diagram calculated from the maxima of $-\partial_V G$, see Fig.4-(d). We note that, although our results point to the existence of three distinct phases, we observe a small drift of the critical value of V_{c1} and V_{c2} with system size. At the present stage, we thus cannot completely rule out that in the infinite system limit the $V_{c1} \rightarrow 0$, *i.e.* ballistic transport only arises at $V = 0$, or even a more dramatic scenario where both $V_{c1}, V_{c2} \rightarrow 0$ and only the diffusive phase is stable for finite V . Although unlikely, disproving these scenarios will require further studies.

Conclusion. — Identifying phases and phase transitions in systems beyond the Landau framework is a challenging task. This situation generically occurs in open quantum systems. We have provided an analysis based on the covariance matrix, which accounts for all single particle correlations, in two specific open quantum systems. Based on this analysis, we have proposed that the affinity susceptibility, and other measures of distance between the single particle correlations matrix, can be used to detect phase transitions where the order parameter is a priori unknown.

In contrast to the well known fidelity susceptibility, these quantities have the advantage of being easily available at a comparatively low computational cost for commonly employed numerical methods, such as Monte-Carlo and MPS techniques. They therefore provide a viable alternative to the fidelity susceptibility for interacting many-body systems where the computation of the fidelity is not feasible.

A remarkable feature of the affinity susceptibility is that in all the cases we studied it signals phase transi-

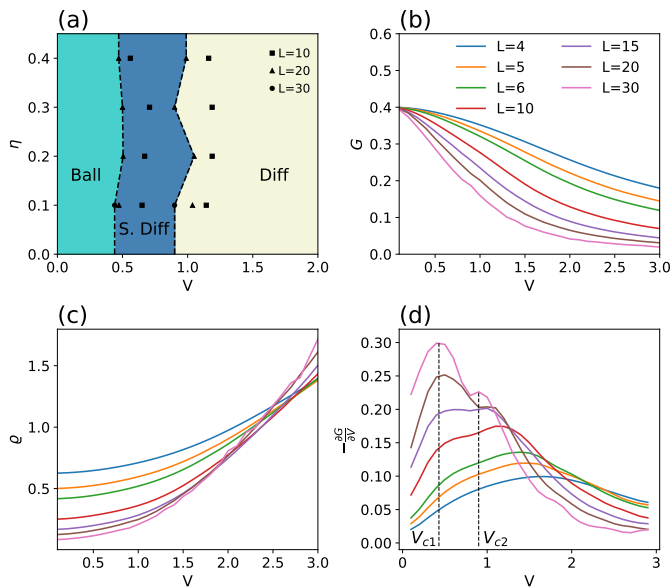


FIG. 4. (a) Phase diagram of the fermion ladder model, showing the presence of ballistic (Ball), diffusive (Diff) and superdiffusive (S. Diff) regimes. For each value of η , boundary lines are based on the largest converged system size. The symbols give the location of the peaks in (d) for different system sizes showcasing the drift of V_{c1} and V_{c2} . (b), (c) and (d) showcase G , ρ and $-\frac{\partial G}{\partial V}$, respectively, as a function of V for different system sizes, for $\eta = 0.1$. In (d) the derivative was obtained numerically using finite differences and the result smoothed with a low-pass filter to remove high-frequency noise.

tions already for comparatively small system sizes. However, it is worth to point out that, perhaps because it also encodes long-range correlations, a higher accuracy is required in the convergence of the MPO as compared to the local operators we studied, like current and density.

In conclusion, we have shown that the affinity susceptibility can be used in practice to identify phase transitions in two illustrative examples. For a boundary driven electronic chain we recovered the known phase diagram and showed that the fidelity susceptibility peaks at the phase transition even for relatively small sizes. For a boundary driven electronic ladder, we used the affinity susceptibility to uncover a non-trivial phase diagram that would naively not be expected based on previous results for spin ladders. This subsequently lead us to confirm the existence of two phase transitions using other signatures, such as the finite size scaling of the current and the spacial density profile.

We gratefully acknowledge Cheng Chen for useful discussions regarding the MPO implementation. Computations were performed on the Tianhe-2JK cluster at the Beijing Computational Science Research Center (CSRC), on the Baltasar-Sete-Sóis cluster, supported by V. Cardoso’s H2020 ERC Consolidator Grant No. MaGRaTh-646597, computer assistance was provided by

CSRC and CENTRA/IST, and on the OBLIVION Supercomputer (based at the High Performance Computing Center - University of Évora) funded by the ENGAGE SKA Research Infrastructure (reference POCI-01-0145-FEDER-022217 - COMPETE 2020 and the Foundation for Science and Technology, Portugal) and by the Big-Data@UE project (reference ALT20-03-0246-FEDER-000033 - FEDER and the Alentejo 2020 Regional Operational Program). M. M. Oliveira acknowledges support by FCT through Grant No. SFRH/BD/137446/2018. MO and PR acknowledge support by FCT through Grant No. UID/CTM/04540/2019. S. K. acknowledges support by the National Key R&D Program of the MOST of China, Grant No. 2016YFA0300202 and the National Science Foundation of China, Grant No. 11774307.

* miguel.m.oliveira@tecnico.ulisboa.pt

† ribeiro.pedro@gmail.com

‡ stefan.kirchner@correlated-matter.com

- [1] S. Morrison and A. S. Parkins, *Phys. Rev. Lett.* **100**, 040403 (2008).
- [2] M. Höning, M. Moos, and M. Fleischhauer, *Phys. Rev. A* **86**, 013606 (2012).
- [3] T. E. Lee, C.-K. Chan, and S. F. Yelin, *Phys. Rev. A* **90**, 052109 (2014).
- [4] S. Genway, W. Li, C. Ates, B. P. Lanyon, and I. Lesanovsky, *Phys. Rev. Lett.* **112**, 023603 (2014).
- [5] D. Manzano and P. I. Hurtado, *Phys. Rev. B* **90**, 125138 (2014).
- [6] H. Wilming, M. J. Kastoryano, A. H. Werner, and J. Eisert, *Journal of Mathematical Physics* **58**, 033302 (2017), <https://doi.org/10.1063/1.4978328>.
- [7] C. Sánchez Muñoz, B. Buča, J. Tindall, A. González-Tudela, D. Jaksch, and D. Porras, *Phys. Rev. A* **100**, 042113 (2019).
- [8] J. S. Ferreira and P. Ribeiro, *Phys. Rev. B* **100**, 184422 (2019).
- [9] J. Huber, P. Kirton, and P. Rabl, *SciPost Phys.* **10**, 45 (2021).
- [10] T. O. Puel, S. Chesi, S. Kirchner, and P. Ribeiro, *Phys. Rev. Lett.* **122**, 235701 (2019).
- [11] J. Hannukainen and J. Larson, *Phys. Rev. A* **98**, 042113 (2018).
- [12] J. Huber, P. Kirton, and P. Rabl, *Phys. Rev. A* **102**, 012219 (2020).
- [13] V. Khemani, A. Lazarides, R. Moessner, and S. L. Sondhi, *Phys. Rev. Lett.* **116**, 250401 (2016).
- [14] D. V. Else, B. Bauer, and C. Nayak, *Phys. Rev. Lett.* **117**, 090402 (2016).
- [15] G. T. Landi, D. Poletti, and G. Schaller, “Non-equilibrium boundary driven quantum systems: models, methods and properties,” (2021), [arXiv:2104.14350 \[quant-ph\]](https://arxiv.org/abs/2104.14350).
- [16] M. Zwołek and G. Vidal, *Phys. Rev. Lett.* **93**, 207205 (2004).
- [17] F. Verstraete, J. J. García-Ripoll, and J. I. Cirac, *Phys. Rev. Lett.* **93**, 207204 (2004).
- [18] T. Prosen and M. Žnidarič, *Journal of Statistical Me-*

- chanics: Theory and Experiment **2009**, P02035 (2009).
- [19] G. Benenti, G. Casati, T. Prosen, and D. Rossini, *EPL (Europhysics Letters)* **85**, 37001 (2009).
- [20] G. Benenti, G. Casati, T. c. v. Prosen, D. Rossini, and M. Žnidarič, *Phys. Rev. B* **80**, 035110 (2009).
- [21] M. Žnidarič, *New Journal of Physics* **12**, 043001 (2010).
- [22] T. c. v. Prosen and M. Žnidarič, *Phys. Rev. Lett.* **105**, 060603 (2010).
- [23] M. Žnidarič, *Phys. Rev. Lett.* **106**, 220601 (2011).
- [24] M. Žnidarič, *Journal of Statistical Mechanics: Theory and Experiment* **2011**, P12008 (2011).
- [25] J. J. Mendoza-Arenas, T. Grujic, D. Jaksch, and S. R. Clark, *Phys. Rev. B* **87**, 235130 (2013).
- [26] J. J. Mendoza-Arenas, S. Al-Assam, S. R. Clark, and D. Jaksch, *Journal of Statistical Mechanics: Theory and Experiment* **2013**, P07007 (2013).
- [27] M. Žnidarič, *Journal of Statistical Mechanics: Theory and Experiment* **2010**, L05002 (2010).
- [28] M. Žnidarič, *Phys. Rev. E* **83**, 011108 (2011).
- [29] T. Prosen, *Phys. Rev. Lett.* **106**, 217206 (2011).
- [30] T. Prosen, *Phys. Rev. Lett.* **107**, 137201 (2011).
- [31] T. Prosen, *Journal of Physics A: Mathematical and Theoretical* **48**, 373001 (2015).
- [32] P. Zanardi, H. T. Quan, X. Wang, and C. P. Sun, *Phys. Rev. A* **75**, 032109 (2007).
- [33] P. Zanardi, L. Campos Venuti, and P. Giorda, *Phys. Rev. A* **76**, 062318 (2007).
- [34] M. Cozzini, R. Ionicioiu, and P. Zanardi, *Phys. Rev. B* **76**, 104420 (2007).
- [35] D. Rossini and E. Vicari, *Phys. Rev. E* **98**, 062137 (2018).
- [36] B. Mera, C. Vlachou, N. Paunković, V. R. Vieira, and O. Viyuela, *Phys. Rev. B* **97**, 094110 (2018).
- [37] See Supplemental Material.
- [38] D. Bures, *Trans. Amer. Math. Soc.* **135**, 199 (1969).
- [39] A. Uhlmann, *Reports on Mathematical Physics* **9**, 273 (1976).
- [40] R. Jozsa, *Journal of Modern Optics* **41**, 2315 (1994), <https://doi.org/10.1080/09500349414552171>.
- [41] A. Uhlmann, *Reports on Mathematical Physics* **36**, 461 (1995), proceedings of the XXVI Symposium on Mathematical Physics.
- [42] H.-P. Breuer and F. Petruccione, *The theory of open quantum systems* (Oxford University Press, 2002).
- [43] C. Gardiner and P. Zoller, *Quantum noise: A Handbook of Markovian and Non-Markovian Quantum Stochastic Methods with Applications to Quantum Optics*, 2nd ed., Springer series in synergetics (Springer, 2000).
- [44] M. Žnidarič, *Phys. Rev. Lett.* **110**, 070602 (2013).
- [45] M. Žnidarič, *Phys. Rev. B* **88**, 205135 (2013).
- [46] T. Prosen and M. Žnidarič, *Phys. Rev. B* **86**, 125118 (2012).
- [47] T. Prosen, *Phys. Rev. Lett.* **112**, 030603 (2014).
- [48] V. Popkov and T. c. v. Prosen, *Phys. Rev. Lett.* **114**, 127201 (2015).
- [49] R. Steinigeweg, F. Heidrich-Meisner, J. Gemmer, K. Michielsen, and H. De Raedt, *Phys. Rev. B* **90**, 094417 (2014).
- [50] A. J. Daley, C. Kollath, U. Schollwöck, and G. Vidal, *Journal of Statistical Mechanics: Theory and Experiment* **2004**, P04005 (2004).
- [51] I. Bengtsson and K. Życzkowski, *Geometry of Quantum States an Introduction to Quantum Entanglement*, 2nd ed. (Cambridge University Press, 2017).
- [52] T. Kailath, *IEEE Transactions on Communication Technology* **15**, 52 (1967).
- [53] D. Dowson and B. Landau, *Journal of Multivariate Analysis* **12**, 450 (1982).
- [54] I. L. C. Michael A. Nielsen, *Quantum Computation and Quantum Information: 10th Anniversary Edition*, 10th ed. (Cambridge University Press, 2011).
- [55] A. H. Werner, D. Jaschke, P. Silvi, M. Kliesch, T. Calarco, J. Eisert, and S. Montangero, *Phys. Rev. Lett.* **116**, 237201 (2016).
- [56] V. V. Albert, B. Bradlyn, M. Fraas, and L. Jiang, *Phys. Rev. X* **6**, 041031 (2016).
- [57] G. Vidal, *Phys. Rev. Lett.* **93**, 040502 (2004).
- [58] T. Prosen and I. Pižorn, *Journal of Physics A: Mathematical and General* **39**, 5957 (2006).
- [59] M. Fishman, S. R. White, and E. M. Stoudenmire, “The ITensor software library for tensor network calculations,” (2020), [arXiv:2007.14822](https://arxiv.org/abs/2007.14822).
- [60] J. S. Ferreira and M. Filippone, *Phys. Rev. B* **102**, 184304 (2020).
- [61] P. Jordan and E. Wigner, *Zeitschrift für Physik* **47**, 631 (1928).
- [62] E. Lieb, T. Schultz, and D. Mattis, *Annals of Physics* **16**, 407 (1961).

— Supplemental Material —

Single-Particle Affinity - a means for detecting Non-equilibrium phase transitions

Miguel M. Oliveira^(a), Pedro Ribeiro^(a,b), and Stefan Kirchner^(c,d)

^(a)CeFEMA, Instituto Superior Técnico, Universidade de Lisboa Av. Rovisco Pais, 1049-001 Lisboa, Portugal

^(b)Beijing Computational Science Research Center, Beijing 100193, China

^(c)Zhejiang Institute of Modern Physics, Zhejiang University, Hangzhou, Zhejiang 310027, China

^(d)Zhejiang Province Key Laboratory of Quantum Technology and Device, Zhejiang University, Hangzhou 310027, China

Summary: Below we provide additional technical details and further numerical results supplementing the conclusions from the main text.

S1. PROPERTIES OF SINGLE-PARTICLE AFFINITY

In this section we present some details regarding how the single-particle affinity is numerically evaluated and show some of its properties. In particular, we demonstrate that the affinity coincides with the mixed-state fidelity for the case of quadratic systems. This allows us to show it satisfies the required properties of a distance between covariance matrices. Finally, we also show that the results in the main text are not tied to the affinity, and should hold for other notions of distance between covariance matrices.

S1.1. Details about the numerical evaluation

The affinity susceptibility is defined in terms of the expansion of the affinity, shown in eq.(2). Defining $\mathcal{A}(\delta) = \mathcal{A}[\Sigma(V), \Sigma(V + \delta)]$, we can write [35, 36]

$$\chi_{VV}(\delta) = -\lim_{\delta \rightarrow 0} \frac{\mathcal{A}(\delta) + \mathcal{A}(-\delta) - 2\mathcal{A}(0)}{\delta^2}. \quad (\text{S1})$$

We evaluate this quantity numerically by fixing the value of the perturbation δ to be small and consider states at points V , $V + \delta$ and $V - \delta$. Note that, since Σ is obtained up to finite numerical precision, the value of δ has to be taken sufficiently large to ensure that the difference between the two covariance matrices is much larger than that precision.

S1.2. Relation with fidelity for free fermions

For quadratic systems the density operator is given by a Gaussian

$$\rho = \frac{1}{Z} e^{-\frac{1}{2} \mathbf{C}^\dagger \Omega \mathbf{C}}, \quad (\text{S2})$$

where $\mathbf{C} = (c_1, \dots, c_L, c_1^\dagger, \dots, c_L^\dagger)^T$ and Ω is a Hermitian matrix with the particle-hole symmetric structure

$$\Omega = \begin{pmatrix} \mathbf{h} & \Delta \\ \Delta^\dagger & -\mathbf{h}^T \end{pmatrix}. \quad (\text{S3})$$

Each of its blocks is a $L \times L$ matrix, with $\mathbf{h} = \mathbf{h}^\dagger$ and $\Delta^T = -\Delta$. For thermal states Ω can be seen as the Hamiltonian divided by temperature. Z is the partition function, which for quadratic models can be written in a simple form

$$Z = \text{Tr} \left[e^{-\frac{1}{2} \mathbf{C}^\dagger \Omega \mathbf{C}} \right] = \sqrt{\det [\mathbf{1} + e^{-\Omega}]} \quad (\text{S4})$$

The covariance matrix also acquires a simple form:

$$\Sigma = \frac{1}{Z} \text{Tr} \left[e^{-\frac{1}{2} \mathbf{C}^\dagger \Omega \mathbf{C}} \mathbf{C} \mathbf{C}^\dagger \right] = [\mathbf{1} + e^{-\Omega}]^{-1} \quad (\text{S5})$$

From the definition of the fidelity

$$F(\rho_1, \rho_2) = \left(\text{Tr} \sqrt{\sqrt{\rho_1} \rho_2 \sqrt{\rho_1}} \right)^2, \quad (\text{S6})$$

and using the identity

$$e^{-\frac{1}{2} \mathbf{C}^\dagger \Omega_1 \mathbf{C}} e^{-\frac{1}{2} \mathbf{C}^\dagger \Omega_2 \mathbf{C}} = e^{-\frac{1}{2} \mathbf{C}^\dagger \tilde{\Omega} \mathbf{C}}, \quad (\text{S7})$$

where $\tilde{\Omega}$ is defined as $e^{-\tilde{\Omega}} = e^{-\Omega_1} e^{-\Omega_2}$, we can write

$$\begin{aligned} F(\rho_1, \rho_2) &= (\text{Tr} \sqrt{\rho_1 \rho_2})^2 \\ &= \frac{1}{Z_1 Z_2} \left(\text{Tr} \sqrt{e^{-\frac{1}{2} \mathbf{C}^\dagger \Omega_1 \mathbf{C}} e^{-\frac{1}{2} \mathbf{C}^\dagger \Omega_2 \mathbf{C}}} \right)^2 \\ &= \frac{1}{Z_1 Z_2} \left(\text{Tr} \sqrt{e^{-\frac{1}{2} \mathbf{C}^\dagger \tilde{\Omega} \mathbf{C}}} \right)^2 \\ &= \frac{1}{Z_1 Z_2} \left(\text{Tr} e^{-\frac{1}{4} \mathbf{C}^\dagger \tilde{\Omega} \mathbf{C}} \right)^2 \\ &= \frac{1}{Z_1 Z_2} \det \left[\mathbf{1} + e^{-\frac{1}{2} \tilde{\Omega}} \right] \\ &= \frac{1}{Z_1 Z_2} \det \left[\mathbf{1} + \sqrt{e^{-\Omega_1} e^{-\Omega_2}} \right] \\ &= \frac{\det \left[\mathbf{1} + \sqrt{(\Sigma_1^{-1} - \mathbf{1}) (\Sigma_2^{-1} - \mathbf{1})} \right]}{\sqrt{\det [\Sigma_1^{-1}] \det [\Sigma_2^{-1}]}} \quad (\text{S8}) \end{aligned}$$

where Σ_i is the covariance matrix corresponding to ρ_i .

Note that in Eq. (S8) we assume that we can invert the covariance matrices. Nevertheless, the expression still has a well defined value in the limit where Σ_i is not invertible.

In this work we extend the applicability of eq. (S8) beyond free systems. This quantity, and others that only depend on the covariance matrix, could in principle be replicated by a system with a quadratic Hamiltonian.

S1.3. Notion of distance for the single-particle affinity

A metric is a function $d : X \times X \rightarrow [0, \infty[$ that provides a distance between two members of some set X . It has to obey the following properties for all $x, y, z \in X$ [51]:

- $d(x, y) = 0 \Leftrightarrow x = y$ identity of indiscernibles
- $d(x, y) = d(y, x)$ symmetry
- $d(x, y) \leq d(x, z) + d(z, y)$ triangle inequality.

The fidelity does not actually constitute a metric between density operators, but it can be related to other quantities that do: the Bures distance $D_B^2(\rho_1, \rho_2) = 2 - 2\sqrt{F(\rho_1, \rho_2)}$ [38–40] and the Bures angle $D_\alpha = \arccos \sqrt{F(\rho_1, \rho_2)}$ [41]. In the previous section we showed how the single-particle affinity corresponds to the fidelity for quadratic systems. By continuation, it follows that it can be related to a notion of distance between states.

S1.4. Other notions of distance

In the main text we focused on the single-particle affinity and its susceptibility to detect out-of-equilibrium phase transitions. To emphasize that the quantity that contains the relevant information is the covariance matrix, we perform here a similar analysis using different notions of distance and verify that the results agree qualitatively with those in the main text.

Consider the Bhattacharyya distance [52] between classical probability distributions $d_{\text{Bhattacharyya}}(p, q) = -\log \int \sqrt{p(x)q(x)} dx$. When evaluated on Gaussian distributions with zero mean, the Bhattacharyya distance writes

$$d_{\text{Bhattacharyya}}(p, q) = \frac{1}{2} \log \left(\frac{\det \frac{C_q + C_p}{2}}{\sqrt{\det C_q \det C_p}} \right), \quad (\text{S9})$$

in terms of the covariance matrices C_p and C_q . This expression induces a distance between real covariant matrices. Its generalisation to Hermitian matrices yields

$$d_{\text{Bhattacharyya}}(\Sigma_1, \Sigma_2) = \frac{1}{2} \log \left(\frac{\det \frac{\Sigma_1 + \Sigma_2}{2}}{\sqrt{\det \Sigma_1 \det \Sigma_2}} \right). \quad (\text{S10})$$

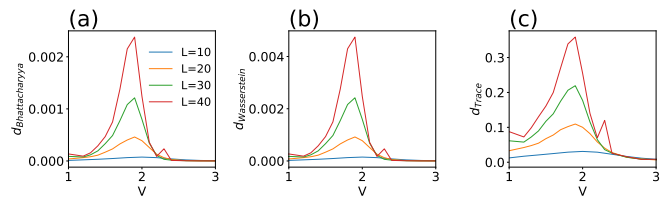


FIG. S1. Shown are alternative notions of distance as a function of V for different system sizes for the fermion chain model. a), b) and c) correspond respectively to the Bhattacharyya, Wasserstein and Trace distances.

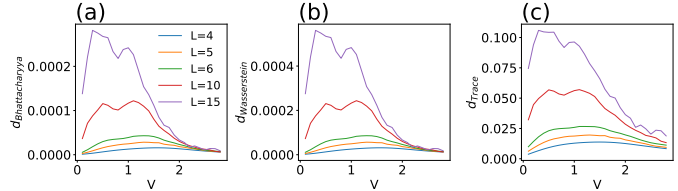


FIG. S2. Alternative notions of distance as a function of V for different system sizes for the fermion ladder model. a), b) and c) correspond respectively to the Bhattacharyya, Wasserstein and Trace distances.

In the same way, from the Wasserstein distance [53] we obtain

$$d_{\text{Wasserstein}}(\Sigma_1, \Sigma_2) = \text{tr} \left[\Sigma_1 + \Sigma_2 - 2\sqrt{\sqrt{\Sigma_2} \Sigma_1 \sqrt{\Sigma_2}} \right]. \quad (\text{S11})$$

Finally, we also consider the Trace distance [54]

$$d_{\text{trace}}(\Sigma_1, \Sigma_2) = \frac{1}{2} \text{tr} |\Sigma_1 - \Sigma_2|, \quad (\text{S12})$$

where $|A| = \sqrt{A^\dagger A}$.

Fig. S1 shows the different distances as a function of V for the chain model while Fig. S2 depicts the ladder case. Both exhibit compatible behavior with the results in Fig. 2 and 3 respectively.

Note that here the distances are computed using only two points, taken at V and $V + \delta V$, which had the effect of slightly left-shifting the results with respect to what was shown in the main text.

S2. BALLISTIC REGIME AT MAXIMAL DRIVING

The $\eta = 1$ states correspond to a configuration of the reservoirs where electrons are only being injected on the left and removed from the right of the system. As mentioned in the main text, even inside the ballistic regime the states at $\eta = 1$ were somewhat special. Even though they still correspond to ballistic behavior, rather than insulating, the SPA peaks as η approaches 1. This can

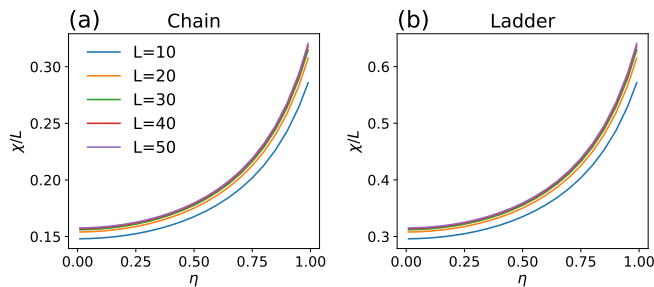


FIG. S3. Affinity susceptibility as a function of η for different system sizes at $V = 0$ for the chain a) and the ladder b). The results were obtained with ED, which for the non-interacting case is numerical efficient, with a perturbation of $\delta\eta = 0.01$.

be seen in Fig.S3-(a) and (b) for the chain and ladder respectively.

S3. OPEN SYSTEMS WITH MPS

Initially developed as a variational approximations for pure states, MPS have been generalized to describe density matrices as Matrix Product Operators (MPO). This allowed for the study of open quantum system and finite temperatures [16, 17]. In this section, we briefly describe the MPS techniques we used to obtain the non-equilibrium steady-states (NESS) for a boundary driven open system described via a Lindblad operator.

A generic density matrix ρ can be written as a MPO as

$$\rho = \sum_{\sigma, \sigma'} M^{\sigma_1, \sigma'_1} \dots M^{\sigma_i, \sigma'_i} \dots M^{\sigma_L, \sigma'_L} |\sigma\rangle \langle \sigma'|, \quad (\text{S13})$$

where $|\sigma\rangle = |\sigma_1 \sigma_2 \dots \sigma_L\rangle$, \sum_{σ} is a sum over all states and L is the system size. M^{σ_i, σ'_i} are the matrices used in the MPO description, with dimension up to D , the so-called bond dimension. Note that for the first and last sites, the M matrices correspond to a row and a column vector respectively, so that the matrix product yields a scalar. Here, the set of σ_i forms a base of the local Hilbert space, with for the models we considered has dimensions 2 for the chain and 4 for the ladder.

A disadvantage of this decomposition is that the parametrization in eq. (S13) does not enforce semi-positiveness of ρ . Since we only analyze the steady-state we have ignored the possible occurrence of unphysical transient regimes at intermediate times. Assuming that the variational wave function can approximate the physical steady-state arbitrarily well, problems with the positivity of the wavefunction can be ignored once the algorithm is well converged.

Although there are algorithms that solve the problem of positivity of the density matrix [55], they entail a

substantial increase in algorithmic complexity and forbid reaching the system sizes attained in the main text.

To obtain the steady-state we initialize the system in an infinite temperature MPO $\rho_0 \propto \mathbb{I}$. This state is then evolved in time until convergence is achieved. To apply the necessary time-evolution operator it is useful to map the state from the space of density matrices to ket space, the so-called Choi-Jamiołkowski isomorphism [56], specified by $\rho \rightarrow |\rho\rangle\rangle$ and $A\rho B \rightarrow A \otimes B^T |\rho\rangle\rangle$. Applied to Eq. (S13) this map boils down to joining the indices σ_i and σ'_i into a single one $s_i = (\sigma_i, \sigma'_i)$, thus yielding a MPS, but with larger local dimension

$$|\rho\rangle\rangle = \sum_{\mathbf{s}} M^{s_1} \dots M^{s_i} \dots M^{s_L} |\mathbf{s}\rangle. \quad (\text{S14})$$

The Lindblad equation, shown earlier in eq. (3), can be rewritten as

$$\partial_t |\rho\rangle\rangle = \hat{\mathcal{L}} |\rho\rangle\rangle \quad (\text{S15})$$

where $\hat{\mathcal{L}}$ is the Lindblad operator, now in the new notation. This looks like a Schrödinger equation with a non-hermitian Hamiltonian. For a time independent problem, *i.e.*, the case considered here, it can be integrated, yielding

$$|\rho(t)\rangle\rangle = e^{\hat{\mathcal{L}}t} |\rho_0\rangle\rangle. \quad (\text{S16})$$

In this form the existing time-evolution algorithms for MPS and unitary dynamics [50, 57] can naturally be applied here without significant modifications [16, 17].

For this work we used the t-DMRG algorithm for time-evolution with a Trotter decomposition of 4th order as described in Ref. [58] and with an associated error per iteration of $O(\Delta t^4)$, where Δt is the time step.

We used the ITensor library [59] as a basis of our implementation. In the initial stages of the evolution a larger time step was chosen, typically in the range $\Delta t \in [0.1, 0.5]$, in order to speed up convergence. In the final stages, when necessary, we switch to a smaller time step to better approximate the steady-state, generally no smaller than $\Delta t = 0.01$.

To guarantee the correctness of the results some care had to be taken regarding the convergence of the obtained steady-states. Not only in time, but convergence in space and with bond dimension also had to be ensured. To achieve this, we followed a similar recipe to the one described in Appendix A of Ref.[60]. For a set of parameters L, V, η and D :

- We monitored J in the middle bond during time-evolution until it saturated. The condition for convergence was $\sigma_t/J_t < 0.01$, where J_t and σ_t are respectively the mean value and the standard deviation of the last 50 values of J obtained during time-evolution. This ensured that fluctuations only affected digits at least 2 decimal places after the most significant one;

- The obtained steady-states are supposed to have a constant current across the length of the system, which was determined by checking if $\sigma_x/J_x < 0.01$, where J_x and σ_x are the mean value and standard deviation for the current at the different bonds. If this condition was not met, the state was evolved further in time until it was met;
- To determine if the MPO description approximates sufficiently well a given steady-state, we also analyzed the convergence with bond dimension. The criterion for convergence of the current with bond dimension, J_D , was $\sigma_D/J_D < 0.01$.

S4. DETAILS ON THE JORDAN-WIGNER TRANSFORMATION

The MPS formalism is more naturally implemented in terms of spin degrees of freedom. Its application to fermionic systems requires adaptations. This is accomplished with the Jordan-Wigner (JW) transformation [61, 62]. For short-range one-dimensional models the Hamiltonian remains local after the transformation and thus amenable to MPS techniques.

The JW transformation is defined as

$$\begin{aligned} c_i &= S_i \sigma_i^- \\ c_i^\dagger &= S_i \sigma_i^+ \end{aligned} \quad (\text{S17})$$

where c_i (c_i^\dagger) are fermionic annihilation (creation) operators, $\sigma^\pm = (\sigma^z \pm i \sigma^y)/2$ are the spin- $\frac{1}{2}$ ladder operators, $\sigma^{x,y,z}$ are the Pauli matrices, and $S_i = \left[\prod_{j=1}^{i-1} (-\sigma_j^z) \right]$ is the string operator.

S4.1. Chain Model

The JW transformation requires an ordering of the sites. For a closed, one-dimensional system the natural sequential ordering yields a local Hamiltonian.

For the chain this yields

$$H = -\frac{t}{2} \sum_{i=1}^{L-1} [\sigma_i^x \sigma_{i+1}^x + \sigma_i^y \sigma_{i+1}^y] + \frac{V}{4} \sum_{i=1}^{L-1} \sigma_i^z \sigma_{i+1}^z. \quad (\text{S18})$$

and

$$\begin{aligned} W_{1,\pm} &= \sqrt{\Gamma_L \frac{1-\eta_L}{2}} \sigma_1^\pm \\ W_{L,\pm} &= \mp \sqrt{\Gamma_R \frac{1-\eta_R}{2}} (-1)^{\hat{N}} \sigma_L^\pm \end{aligned} \quad (\text{S19})$$

where we used in the expression for $W_{L,\pm}$ that $S_{L-1} \sigma_L^\pm = \mp (-1)^{\hat{N}} \sigma_L^\pm$ where \hat{N} counts the number of occupied fermion states (or spins up).

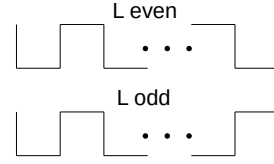


FIG. S4. Jordan-Wigner ordering for the fermion ladder.

We now have to consider the effect of the $(-1)^{\hat{N}}$ operator on the Lindblad equation, see Eq.(4). The only non-trivial term is the one where the jump operator acts from both the left and the right. To deal with this it is helpful to consider that the density matrix has two sectors that are not mixed by the Lindblad equation, the $\{|even\rangle\langle even|, |odd\rangle\langle odd|\}$ and $\{|even\rangle\langle odd|, |odd\rangle\langle even|\}$. The operator $(-1)^{\hat{N}}$ commutes with the former and anti-commutes with the later, so we can replace it with 1 and -1 respectively. Expectation values of operators composed of an even number of creation and annihilation operators only have contributions from the first sector of the density matrix, therefore, we consider only this sector.

S4.2. Ladder Model

For the fermion ladder model, regardless of the choice of ordering, the string operator always leads to the appearance of additional interaction terms in the spin model.

For the results in the main text, we chose the zig-zag ordering in Fig.S4, which maintained the locality of the Hamiltonian. As suggested by the picture, nearest neighbor sites can have string operators in the intra-chain hopping terms, depending on whether the corresponding bond is even or odd.

For clarity, instead of giving the transformed spin Hamiltonian and jump operators we list below the transformation rules from fermionic operators to spins.

Labeling the rungs by $\tau = 1, 2$ for the upper and lower chain respectively, the intra-chain hopping terms of the Hamiltonian in Eq. (5) transform according to

$$\begin{aligned} c_{i,\tau}^\dagger c_{i+1,\tau} &\rightarrow \sigma_{i,\tau}^+ \sigma_{i+1,\tau}^- \\ c_{i+1,\tau}^\dagger c_{i,\tau} &\rightarrow \sigma_{i,\tau}^- \sigma_{i+1,\tau}^+ \\ c_{i,\bar{\tau}}^\dagger c_{i+1,\bar{\tau}} &\rightarrow \sigma_{i,\bar{\tau}}^+ \sigma_{i,\tau}^z \sigma_{i+1,\tau}^- \sigma_{i+1,\bar{\tau}}^- \\ c_{i+1,\bar{\tau}}^\dagger c_{i,\bar{\tau}} &\rightarrow \sigma_{i,\bar{\tau}}^- \sigma_{i,\tau}^z \sigma_{i+1,\tau}^z \sigma_{i+1,\bar{\tau}}^+ \end{aligned} \quad (\text{S20})$$

For an even bond we have that $\tau = 1$ and $\bar{\tau} = 2$, and for an odd bond $\tau = 2$ and $\bar{\tau} = 1$. For the inter-chain hopping and interaction terms the corresponding operators

transform as

$$\begin{aligned} c_{i,\tau}^\dagger c_{i,\bar{\tau}} &\rightarrow \sigma_{i,\tau}^+ \sigma_{i,\bar{\tau}}^- \\ c_{i,\tau}^\dagger c_{i,\tau} - 1/2 &\rightarrow \sigma_{i,\tau}^z/2. \end{aligned} \quad (\text{S21})$$

Using the same reasoning as for the chain model, we can obtain the transformation rules for the jump operators. For the left side of the ladder we get

$$\begin{aligned} c_{1,1} &\rightarrow \sigma_{1,1}^- \\ c_{1,1}^\dagger &\rightarrow \sigma_{1,1}^+ \\ c_{1,2} &\rightarrow \sigma_{1,1}^z \sigma_{1,2}^- \\ c_{1,2}^\dagger &\rightarrow \sigma_{1,1}^z \sigma_{1,2}^+. \end{aligned} \quad (\text{S22})$$

On the right side we obtain

$$\begin{aligned} c_{L,\tau} &\rightarrow \sigma_{L,\tau}^- \\ c_{L,\tau}^\dagger &\rightarrow \sigma_{L,\tau}^+ \\ c_{L,\bar{\tau}} &\rightarrow \sigma_{L,\tau}^z \sigma_{L,\bar{\tau}}^- \\ c_{L,\bar{\tau}}^\dagger &\rightarrow \sigma_{L,\tau}^z \sigma_{L,\bar{\tau}}^+, \end{aligned} \quad (\text{S23})$$

where for L even we have $\tau = 1$ and $\bar{\tau} = 2$, and for L odd $\tau = 2$ and $\bar{\tau} = 1$.

S4.3. Observables

In this subsection, it is shown how to relate the spin and fermionic observables used to characterize the different NESS regimes.

1. Occupation

The local occupation transform according to

$$\langle n_i \rangle = \frac{\langle \sigma_i^z \rangle + 1}{2}, \quad (\text{S24})$$

which is valid for both the chain and ladder models.

2. Current

The current operator in the chain model is written in terms of the spin degrees of freedom as

$$J_i^{\text{chain}} = -\frac{t}{2} \langle \sigma_i^x \sigma_{i+1}^y - \sigma_i^y \sigma_{i+1}^x \rangle. \quad (\text{S25})$$

For the ladder one finds

$$\begin{aligned} J_i^{\text{ladder}} &= -\frac{t}{2} \langle \sigma_{i,\tau}^x \sigma_{i+1,\tau}^y - \sigma_{i,\tau}^y \sigma_{i+1,\tau}^x \rangle \\ &\quad - \frac{t}{2} \langle \sigma_{i,\bar{\tau}}^x \sigma_{i,\tau}^z \sigma_{i+1,\tau}^z \sigma_{i+1,\bar{\tau}}^y - \sigma_{i,\bar{\tau}}^y \sigma_{i,\tau}^z \sigma_{i+1,\tau}^z \sigma_{i+1,\bar{\tau}}^x \rangle, \end{aligned} \quad (\text{S26})$$

where $\tau = 1$ and $\bar{\tau} = 2$ for an even bond, and $\tau = 2$ and $\bar{\tau} = 1$ for an odd one.

3. Covariance Matrix

Consider the block decomposition of the covariance matrix

$$\Sigma = \begin{pmatrix} \langle cc^\dagger \rangle & \langle cc \rangle \\ \langle c^\dagger c^\dagger \rangle & \langle c^\dagger c \rangle \end{pmatrix}. \quad (\text{S27})$$

The first block is given by

$$\langle c_i c_j^\dagger \rangle = \langle \sigma_i^- S_{i,j} \sigma_j^+ \rangle, \quad (\text{S28})$$

where we assumed, without loss of generality, that $i < j$ and $S_{i,j} = \left[\prod_{k=i}^{j-1} (-\sigma_k^z) \right]$. The other cases can be obtained by taking advantage of the symmetries of the covariance matrix. The string operator for the chain will be a straight line between the sites i and j , whereas for the ladder it will be a zig-zag line, see Fig.S4.